Available online at www.sciencedirect.com
ScienceDirect
Polymer 47 (2006) 8480–8487
polymer
www.elsevier.com/locate/polymer

Reverse micelles of star-block copolymer as nanoreactors for preparation of gold nanoparticles

Junbo Li, Linqi Shi*, Yingli An, Yan Li, Xi Chen, Huijun Dong

Key Laboratory of Functional Polymer Materials, Ministry of Education, Institute of Polymer Chemistry, College of Chemistry, Nankai University, No. 94, Weijin Road, Nankai District, Tianjin 300071, China

Received 20 June 2006; received in revised form 18 August 2006; accepted 24 September 2006
Available online 7 November 2006

Abstract

The star-block copolymers poly(styrene)-*block*-poly(4-vinylpyridine) ((PS-*b*-P4VP)$_4$) are synthesized by two-step atom transfer radical polymerization (ATRP) using pentaerythritol tetrakis (2-bromoisobutyrate) as initiator. The star-block copolymers form reverse micelles in toluene with the P4VP core and the PS shell. The reverse micelles and their complexes with $HAuCl_4 \cdot 3H_2O$ are investigated by a combination of dynamic laser scattering (DLS) and static laser scattering (SLS) in toluene. Gold nanoparticles are subsequently obtained by reducing the complex micelles with anhydrous hydrazine. The size and morphology of reverse micelles, hybrid micelles and gold nanoparticles are also investigated by transmission electron microscope (TEM). The obtained gold nanoparticles are of small quantum size (ca. 2 nm) and narrow distribution.

Keywords: Star-block copolymers; Reverse micelles; Gold nanoparticles

1. Introduction

Amphiphilic block copolymers in selective solvent can form well-defined micelles with the insoluble block as the core and the soluble block as the shell or corona. These micelle systems have the potential and practical application such as drug delivery [1,2], microreactors [3], and general detergents [4]. A further advancement of these techniques is to prepare nanoparticles to produce hybrid materials [5–7] made up of polymer and inorganics. In recent years, the study on gold nanoparticles has attracted more and more interest since gold nanoparticles with quantum size (<10 nm) have demonstrated high catalytic activity for both oxidation and reduction reactions [8]. Therefore, designing of new polymeric micelle system for the synthesis of well-defined nanomaterials with controlled dimensions and morphology will be one of the most important challenges both for academic and applicational reasons. Eisenberg's group [9] studied micellization of a poly(ethylene oxide)-*block*-poly(4-vinylpyridine) (PEO-*b*-P4VP) copolymer complex with three types of gold compounds $NaAuCl_4$, $HAuCl_4$, and $AuCl_3$ in water. Möller and coworkers [10,11] successfully prepared uniform gold nanoparticles and arranged them spatially in two-dimensional arrays by using poly(styrene)-*block*-poly(2-vinylpyridine) (PS-*b*-P2VP) diblock copolymer micelles. Wang et al. [12] prepared polyelectrolyte-protected gold nanoparticles through one-step thermal process. Mays et al. [13] and Schubert et al. [14] prepared gold nanoparticles in unimolecular micelles of PS-*b*-P2VP and poly(ethylene oxide)-*block*-poly(ε-caprolactone) (PEO-*b*-PCL) star-block copolymers, respectively. McFarland and his coworkers [15] got gold nanoparticles with the diameters between 1.5 and 6 nm and found that the smallest particles (1.5 nm) are the most active for electro-oxidation to CO.

Star polymers [16], with polymer chains being combined at a single branch point, have attracted much attention due to

* Corresponding author. Tel.: +86 22 23501945; fax: +86 22 23503510.
E-mail address: shilinqi@nankai.edu.cn (L. Shi).

0032-3861/$ - see front matter © 2006 Elsevier Ltd. All rights reserved.
doi:10.1016/j.polymer.2006.09.071

their branched structures and unique physicochemical properties. Block-arm star copolymer of $(AB)_n$ type has n diblock junctions on a common point and has a natural ''core–shell'' type molecular structure [13] by the self-micellization. This polymer has special molecular structure and is widely used to prepare the peculiar unimolecular micelle [17]. However, the reverse micelles of these polymers [18–20] (namely the outside block (far from molecular center) as the core and the inner block (close to molecular center) as the corona) and their application as nanoreactors for preparation of metal nanoparticles are seldom reported.

Here, we synthesize (PS-*b*-P4VP)$_4$ (where 4 is the number of arm) of low polydispersity index (PDI) with different chain length of P4VP by atom transfer radical polymerization (ATRP). (PS-*b*-P4VP)$_4$ forms reverse micelles in toluene with P4VP as the core and PS as petal-like shell. The reverse micelles and micelles complex with $HAuCl_4 \cdot 3H_2O$ are investigated by means of dynamic laser scattering (DLS) and static laser scattering (SLS), respectively. After reducing the complex micelles, we obtain gold nanoparticles of small particle size (ca. 2 nm), identical particle morphology and narrow distribution (transmission electron microscope (TEM)).

2. Experimental section

2.1. Materials

THF (Aldrich, AR) is distilled from a purple sodium ketyl solution. Triethylamine (Aldrich, AR) is stirred over magnesium sulfate and filtered just prior to use. Styrene and 4-vinylpyridine (Acros Organics, AR) are distilled from calcium hydride. CuBr and CuCl are synthesized in our laboratory. Tris[2-(dimethylamino)ethyl]amine (Me_6TREN) is synthesized from tris(2-amino)ethyl amine (TREN) (Acros Organics, AR) [21]. Bipyridine (BPY) (Aldrich, AR), 2-bromoisobutyryl bromide (Acros Organics, AR), sodium hydroxide (Aldrich, AR) and pentaerythritol (Acros Organics, AR), are used as received.

2.2. Synthesis of pentaerythritol tetrakis (2-bromoisobutyrate) (4Bri-Bu)

4Bri-Bu is synthesized according to Ref. [22]. A 3.7 g (27 mmol) sample of pentaerythritol and 12 g (0.12 mol) triethylamine are solved into a 250 mL round-bottom flask with 125 mL of THF. A solution containing 26 g (0.12 mol) of bromopropionyl bromide and 20 mL THF are added to a 50 mL pressure equalizing addition funnel fitted to the flask under Ar (g). The reactor is cooled to 0 °C in an ice/water bath, and the acid halide solution is added dropwise. The reaction is stirred overnight and allowed to warm to room temperature of its own accord. The mixture is transferred to a 1 L separatory funnel with 300 mL of diethyl ether and extracted consecutively with 200 mL of H_2O, 3 × 200 mL of $NaHCO_3$ (aq), and 200 mL of H_2O. The organic phase is dried over $MgSO_4$ and filtered and the solvent removed by rotary evaporation. The product, a white solid, is recrystallized twice from the diethyl ether phase, isolated and recrystallized again from diethyl ether. ^{1}H NMR ($CDCl_3$) δ: 4.31 (s, 8H, C–CH_2–O), 1.93 (s, 24H, C (Br)–CH_3) ppm.

2.3. Synthesis of star macroinitiators (PS-Br)$_4$

Four-arm star macroinitiators (PS-Br)$_4$ are synthesized by ATRP [23]. 4Bri-Bu (2.0 g) is added to a reaction flask, and then CuBr and BPY catalysts are introduced into the reaction flask. At last, 20.0 g of styrene is added into the flask and degassed under nitrogen purge. Polymerization is performed at 120 °C for 6 h and the monomer conversion in 6 h is over 75%. The polymer (PS-Br)$_4$ is purified by first passing through a Al_2O_3 column to remove the copper catalyst and then deposited in alcohol.

2.4. Synthesis of the star-block copolymer (PS-b-P4VP)$_4$

The typical polymerization procedure is as follows: 2.0 g (PS-Br)$_4$ and 2 mL solvent mixture of butanone and 2-propanol (7:3 by volume) are added to a reaction flask. The sample is stirred and then degassed under nitrogen purge. Subsequently, 0.1 g CuCl, 0.22 g Me_6TREN and certain weight 4-vinylpyridine are introduced into the reaction flask and degassed under nitrogen purge again. Polymerization is performed at 40 °C for 4 h and the monomer conversion is over 80%. Star-block copolymer (PS-*b*-P4VP)$_4$ is purified by first passing through the Al_2O_3 column to remove the copper catalyst and then deposited in cold ether. The powder of (PS-*b*-P4VP)$_4$ is dried in a vacuum oven at 40 °C. The synthesis procedures are illustrated in Scheme 1.

2.5. Preparation of the (PS-b-P4VP)$_4$ micelles

Star-block copolymers (PS-*b*-P4VP)$_4$ with different length of P4VP chains are first dissolved in CH_2Cl_2 to prepare polymer solution with an initial concentration of 2.0 mg/mL. Subsequently, a given volume of toluene is added into the polymer solution with stirring. As the solution turns turbidity, (PS-*b*-P4VP)$_4$ micelles are formed. After 2 h, toluene is added until the concentration is 0.20 mg/mL. The micelle solution is kept overnight and then heated in a thermostatic bath at 42 °C for 5 h to remove CH_2Cl_2. Certain volume of toluene is added into the micelles solution to keep the total volume unchanged. The micelle solution is kept overnight and then diluted with toluene to 0.1 mg/mL for LS measurements.

2.6. Preparation of the complex micelles

To prepare complex micelles, 0.2 mg/mL of the obtained micelle solutions is mixed with 0.5 equiv of $HAuCl_4 \cdot 3H_2O$ per pyridine unit. $HAuCl_4 \cdot 3H_2O$ is insoluble in toluene but may be incorporated into the micelles cores by coordinating with 4VP units. Thus, the solutions of complex micelles are obtained after the mixtures were stirred over 24 h. The solutions of complex micelles are also diluted with toluene to 0.1 mg/mL for LS measurements.

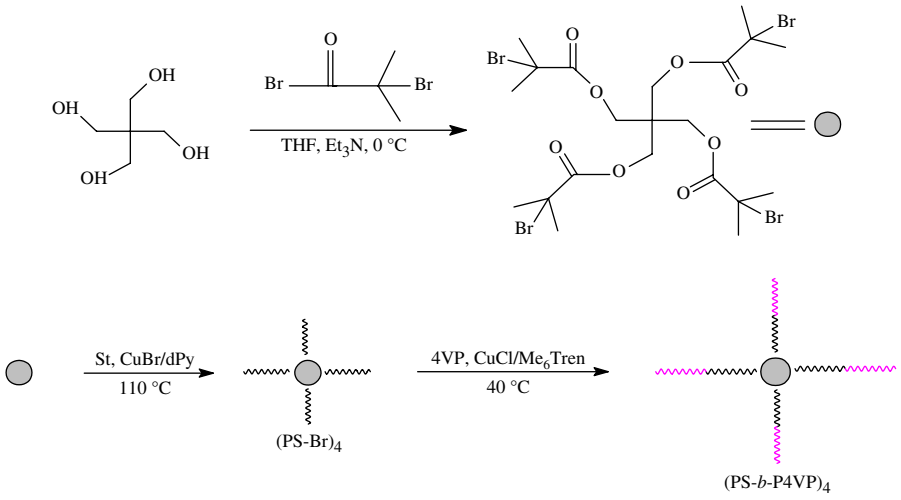

Scheme 1. Schematic representation for the synthesis of (PS-*b*-P4VP)$_4$.

2.7. Preparation of gold nanoparticles

Excess solution (0.02 vol%) of anhydrous N_2H_4 (prepared based on Ref. [10]) in toluene is added dropwise into 10 mL (0.2 mg/mL) solutions of complex micelles. After 24 h, aqueous HCl (38%) is added to the solution to remove the excess N_2H_4.

2.8. Characterization

The ^{1}H NMR spectra of the polymers in $CDCl_3$ are recorded on a Bruker AV300 spectrometer operating at 300 MHz for protons. PDI are characterized by a Waters 600E gel permeation chromatography (GPC) analysis system equipped with Waters 2414 refractive index detector at 30 °C, Waters 1515 isocratic HPLC pump and waters styragel HT columns, where *N*,*N*-dimethylformamide (DMF) is used as the eluent at a flow rate of 1.0 mL/min and linear polystyrene as the calibration standard. Transmission electron microscopy (TEM) is conducted by using a Philips T20ST electron microscopy at an acceleration voltage of 200 kV. Thin films are prepared by dipping a drop of the solution onto a carbon-coated copper grid and then volatilizing the solution at room temperature. UV–vis absorption spectrum is obtained using a Perkin–Elmer UV–vis spectrometer (Lambda 20).

All these samples are filtered through a 0.45 μm Millipore filter into a clean scintillation vial and characterized by a combination of dynamic (DLS) and static (SLS) laser scatterings. In this study, DLS and SLS measurements are performed on a laser light scattering spectrometer (BI-200SM) equipped with a digital correlator (BI-9000AT) at 532 nm. All LS measurements are performed at 25 °C. The detailed method of LS measurement refers to our recent works or Wu's study [24].

3. Results and discussion

3.1. Characterization of (PS-Br)$_4$ and (PS-b-P4VP)$_4$

ATRP has been successfully proven to be very efficient to prepare well-defined star polymers with regular stars and precise arm numbers [25,26]. Here, we synthesize star-block copolymer of (PS-*b*-P4VP)$_4$ by two-step ATRP. The GPC traces of macromolecular initiator and star-block copolymers are shown in Fig. 1. The low PDI indicates that molecular mass distribution is narrow. The composition of (PS-Br)$_4$ and (PS-*b*-P4VP)$_4$ is determined by ^{1}H NMR spectra, which is shown in Fig. 2. (PS-Br)$_4$ is determined by the ratio of the total area of peaks e and d to peak b. The composition of (PS-*b*-P4VP)$_4$ is determined by the ratio of the total area of peaks f and d to peak b. The detailed data of characteristics are summarized in the Table 1.

3.2. The LS of reverse micelles and complex micelles

As described in Section 2, toluene is a block-selective solvent for PS but a precipitant for P4VP. The core–shell micelles of (PS-*b*-P4VP)$_4$ with different length of P4VP chains are produced by adding toluene into the CH_2Cl_2 solution of (PS-*b*-PVP)$_4$ and the structure of the micelle is kinetically frozen as CH_2Cl_2 is removed from the solution, with P4VP chains (external block) as the core and PS chains (inner block) as the petal-like shell [18,20]. Compared with the brush-like

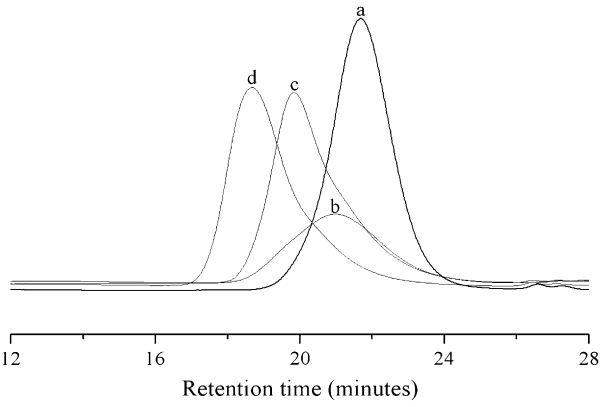

Fig. 1. GPC traces for: (a) (PS$_{25}$-Br)$_4$, (b) (PS$_{25}$-*b*-P4VP$_{17}$)$_4$, (c) (PS$_{25}$-*b*-P4VP$_{37}$)$_4$ and (d) (PS$_{25}$-*b*-P4VP$_{63}$)$_4$ in DMF at room temperature.

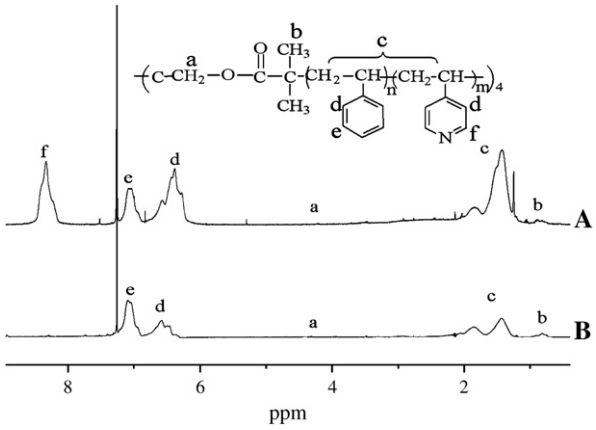

Fig. 2. ^{1}H NMR spectra of (PS-Br)$_4$ and (PS-*b*-P4VP)$_4$.

Table 1
Characteristics of the synthesized polymers

Samples	$M_{n,\mathrm{th}}$ (g/mol)[a]	PDI[b]	$M_{n,\ ^1\mathrm{H\ NMR}}$ (g/mol)[c]	Yield (%)[d]
$(PS_{25})_4$	1.2×10^4	1.16	1.0×10^4	85
$(PS_{25}$-*b*-$P4VP_{17})_4$	2.0×10^4	1.27	1.7×10^4	70
$(PS_{25}$-*b*-$P4VP_{37})_4$	3.0×10^4	1.30	2.5×10^4	83
$(PS_{25}$-*b*-$P4VP_{63})_4$	4.0×10^4	1.38	3.5×10^4	88

[a] Calculated by the monomer conversion is 100%.
[b] Measured by GPC.
[c] Calculated by ^{1}H NMR.
[d] Determined by gravimetric method.

shell of the micelle formed by diblock copolymer, this shell has a restricted and closed structure because the *n* chains of the same copolymer spread from the core and join at a single point. $HAuCl_4 \cdot 3H_2O$ is incorporated into the micellar core by forming complex with the 4VP units. Gold nanoparticles are subsequently obtained by reducing the complex micelles with anhydrous hydrazine. The forming process of the micelle, complex micelle and gold nanoparticle is shown in Scheme 2.

The self-assembling behaviors of the micelles and the complex micelles are investigated by DLS and SLS in toluene,

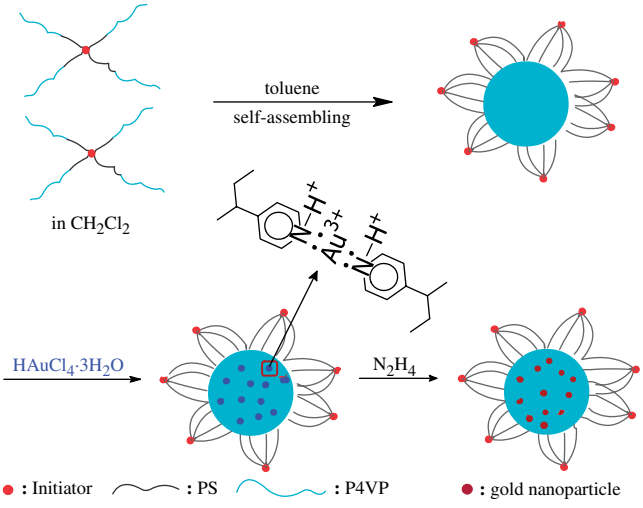

Scheme 2. Schematic representation for the preparation of reversed micelles and gold nanoparticles.

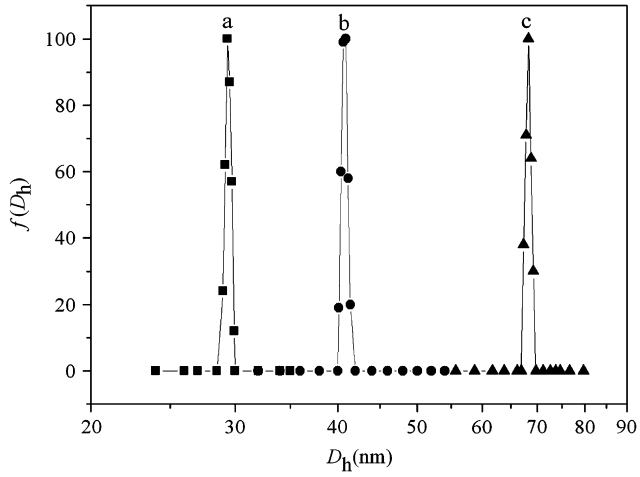

Fig. 3. Hydrodynamic diameter distribution $f(D_h)$ of micelles: (a) $(PS_{25}$-*b*-$P4VP_{17})_4$, (b) $(PS_{25}$-*b*-$P4VP_{37})_4$ and (c) $(PS_{25}$-*b*-$P4VP_{63})_4$. The polymer concentration is 0.1 mg/mL. All DLS measurements are performed at scattering angle 90° at 25 °C.

respectively. Fig. 3 shows the hydrodynamic diameter distribution, $f(D_h)$, of the micelles formed by $(PS_{25}$-*b*-$P4VP_{17})_4$, $(PS_{25}$-*b*-$P4VP_{37})_4$ and $(PS_{25}$-*b*-$P4VP_{63})_4$. The relative width μ_2/Γ^2 measured by DLS are 0.08, 0.07 and 0.1. Clearly, the micelles are much narrowly distributed.

Fig. 4 shows the plot of the translational diffusion coefficient (D) versus q^2 of the reverse micelles. The values of D of the micelles are essentially independent of q^2, which suggests that the micelles are uniformly spherical [27]. From the fitted line in Fig. 4, the translational diffusion coefficient (D^0) calculated by extrapolating q^2 to 0 is 2.97×10^7 cm^2/s, 1.76×10^7 cm^2/s and 0.95×10^7 cm^2/s, respectively. The D_hs of the micelles are 26.4, 44.3 and 74 nm, respectively, which are calculated according to Stokes–Einstein equation $D_h = k_bT/(3\pi\eta D)$, where k_b, T, and η are the Boltzmann constant, the absolute temperature and the solvent viscosity. The D_hs of the micelle increase with increasing length of the P4VP

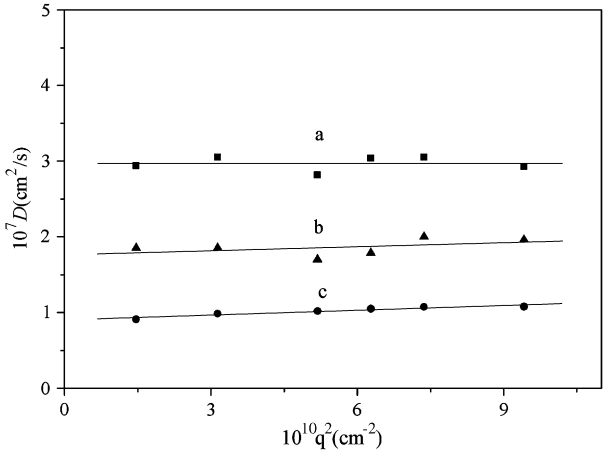

Fig. 4. Plot of D vs q^2 of the micelles: (a) $(PS_{25}$-*b*-$P4VP_{17})_4$, (b) $(PS_{25}$-*b*-$P4VP_{37})_4$ and (c) $(PS_{25}$-*b*-$P4VP_{63})_4$. The polymer concentration is 0.1 mg/mL. All DLS measurements are performed at 25 °C.

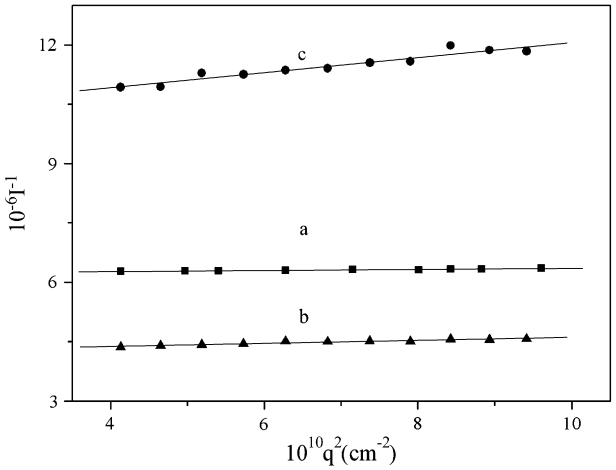

Fig. 5. Berry plot of I^{-1} vs q^2 of the micelles: (a) $(PS_{25}$-b-$P4VP_{17})_4$, (b) $(PS_{25}$-b-$P4VP_{37})_4$ and (c) $(PS_{25}$-b-$P4VP_{63})_4$. The polymer concentration is 0.1 mg/mL.

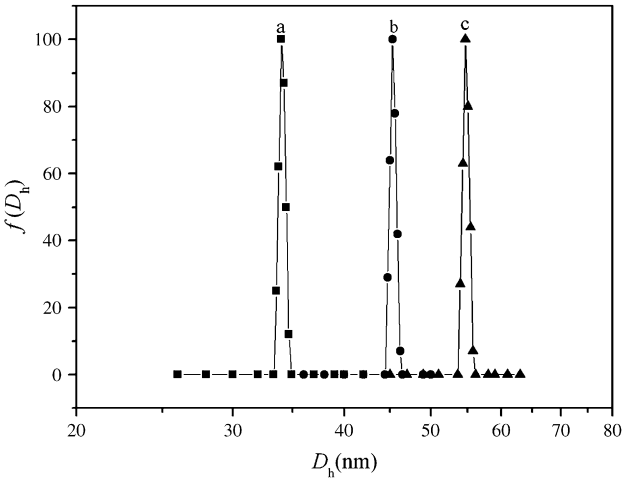

Fig. 6. Hydrodynamic diameter distribution $f(D_h)$ vs q^2 of complex micelles with 0.5 equiv of $HAuCl_4 \cdot 3H_2O$ per pyridine unit: (a) $(PS_{25}$-b-$P4VP_{17})_4$, (b) $(PS_{25}$-b-$P4VP_{37})_4$ and (c) $(PS_{25}$-b-$P4VP_{63})_4$. The polymer concentration is 0.1 mg/mL. All DLS measurements are performed at scattering angle 90° at 25 °C.

block, such a trend agrees well with that of the micelles formed by PS-*b*-P4VP in Refs. [28,29].

Fig. 5 shows the Berry plots of I^{-1} of the micelles versus q^2, where I is the scattering intensity of the sample at a scattering angle θ. From each line fitted in Fig. 5, the apparent gyration radius R_g of the micelles are calculated according to $R_g = (3S/T)^{0.5}$ [30], where S is the slope and T is the intercept. The calculated values of R_g are 8.4, 13.6 and 30.4 nm. It is known that the R_g/R_h value reveals the morphology of particles in solution. For a uniform nondraining sphere, a hyperbranched cluster, and a random coil the ratios of R_g/R_h are 0.774, 1.0–1.3, and 1.5–1.8, respectively [31]. The R_g/R_h values of the micelles formed by $(PS_{25}$-b-$P4VP_{17})_4$ and $(PS_{25}$-b-$P4VP_{37})_4$ are 0.64 and 0.61(<0.775), respectively, which indicates that the core of the micelles are dense. For micelles formed by $(PS_{25}$-b-$P4VP_{63})_4$, the R_g/R_h value is 0.82(>0.775), indicating the core of micelle is a relatively loose core. It is reported that the cylindrical morphology of PS-*b*-P4VP is formed at high R_g/R_h value (0.803) [28]. In the present case, the morphology of the micelles formed by $(PS_{25}$-b-$P4VP_{63})_4$ still keeps spherical at R_g/R_h 0.82. The closed and dense structure of petal-like shells has efficiently prohibited the contact of the P4VP between the two adjacent micelles, and further prevented the coalescence of micelles to form bigger aggregates.

Figs. 6 and 7 show the plot of $f(D_h)$ and D versus q^2 of the complex micelles. All the $f(D_h)$ still shows narrow distribution, and the values of D of the micelles are essentially independent of q^2, also indicating that the complex micelles still keep the regular spherical morphology. The D_hs of the micelles are 39, 51.5 and 59 nm (Fig. 7).

The Berry plot of I^{-1} of the micelles versus q^2 is shown in Fig. 8, the R_gs are 20.7, 21.3 and 23.9 nm. The R_g/R_h of the complex micelles is calculated as 1.06, 0.83 and 0.81.

The detailed data of DLS and SLS are summarized in Table 2. From Table 2, it could be found that as $HAuCl_4 \cdot 3H_2O$ was incorporated into the core of the reverse micelles, the D_h of the reverse micelle of $(PS_{25}$-b-$P4VP_{17})_4$ and $(PS_{25}$-b-$P4VP_{37})_4$ increases about 12.6 and 7.2 nm, while the D_h of

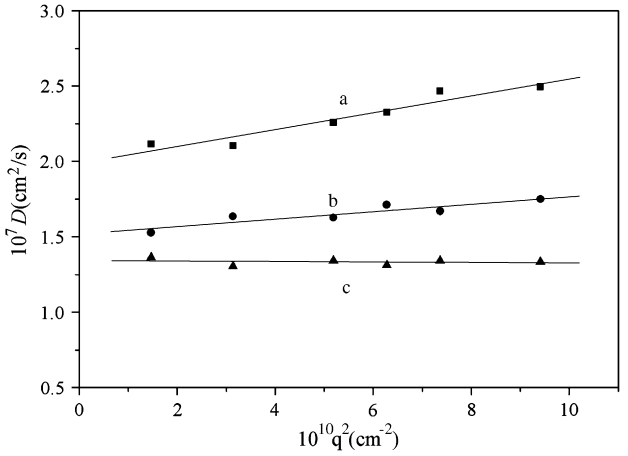

Fig. 7. Plot of D vs q^2 of the complex micelles with 0.5 equiv of $HAuCl_4 \cdot 3H_2O$ per pyridine unit: (a) $(PS_{25}$-b-$P4VP_{17})_4$, (b) $(PS_{25}$-b-$P4VP_{37})_4$ and (c) $(PS_{25}$-b-$P4VP_{63})_4$. The polymer concentration is 0.1 mg/mL. All DLS measurements are performed at 25 °C.

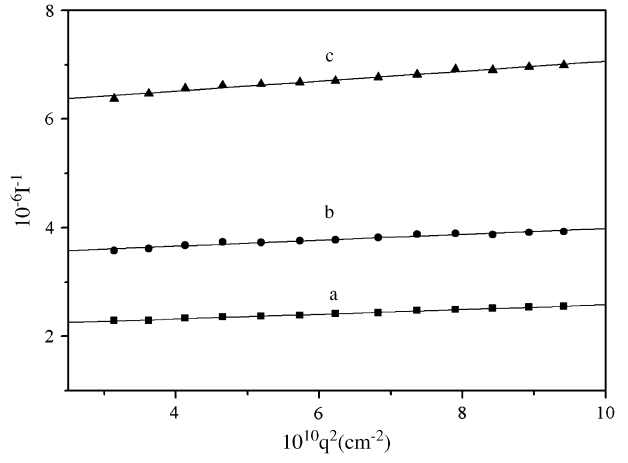

Fig. 8. Berry plot of I^{-1} vs q^2 of the complex micelles with 0.5 equiv of $HAuCl_4 \cdot 3H_2O$ per pyridine unit: (a) $(PS_{25}$-b-$P4VP_{17})_4$, (b) $(PS_{25}$-b-$P4VP_{37})_4$ and (c) $(PS_{25}$-b-$P4VP_{63})_4$. The polymer concentration is 0.1 mg/mL.

Table 2
Detailed data of DLS and SLS

Samples	D_h (nm)	R_g (nm)	R_g/R_h	D_h^{com} (nm)	R_g^{com} (nm)	R_g/R_h^{com}
$(PS_{25}$-*b*-$P4VP_{17})_4$	26.4	8.4	0.64	39.0	20.7	1.06
$(PS_{25}$-*b*-$P4VP_{37})_4$	44.3	13.6	0.61	51.5	21.3	0.83
$(PS_{25}$-*b*-$P4VP_{63})_4$	74.0	30.4	0.82	59.0	24.0	0.81

D_h, R_g and R_g/R_h are data of the reverse micelles and D_h^{com}, R_g^{com} and R_g/R_h^{com} are data of complex micelles.

the reverse micelle decreases 15 nm for $(PS_{25}$-*b*-$P4VP_{63})_4$; the corresponding R_gs increase about 12.3 and 7.7 nm for micelles of $(PS_{25}$-*b*-$P4VP_{17})_4$ and $(PS_{25}$-*b*-$P4VP_{37})_4$, while decreases 10.4 nm for $(PS_{25}$-*b*-$P4VP_{63})_4$. The change of R_g/R_h has a same trend with D_h and R_g. The distinct changes can be attributed to two factors. First, after $HAuCl_4 \cdot 3H_2O$ is incorporated into the core of the micelle, most of 4VP units are protonated and form a polyionic block [13,32]. The electrostatic repulsion among polyionic blocks leads to increase in the size of the core. On the other hand, Au atom of $HAuCl_4 \cdot 3H_2O$ will chelate [33] with two or more N atoms of 4VP unit as a crosslink point, which makes micellar core shrinking and the density of the core increasing [9]. Two factors simultaneously influence the sizes of the micelles, for a dense core formed by $(PS_{25}$-*b*-$P4VP_{17})_4$ and $(PS_{25}$-*b*-$P4VP_{37})_4$, the electrostatic repulsion is predominant, leading to a relative loose core. However, for a loose micellar core formed by $(PS_{25}$-*b*-$P4VP_{63})_4$, the chelation is predominant and lead to the decrease of the size of the micelles.

3.3. Characterization of gold nanoparticles

UV–vis absorption spectra of the gold nanoparticles are presented in Fig. 9. The three absorption bands at ~525 nm are assigned to the surface plasmon resonance of small gold nanoparticles [34]. Although the gold nanoparticles are produced in the different size of the core micelles, the location of absorption bands is less than 5 nm, which indicates gold nanoparticles have the relative uniform size. Their intensity increased with increasing number of 4VP units.

The TEM images of the micelle and its gold nanoparticle are shown in Fig. 10. All the micellar aggregates are uniform sphere (see Fig. 10a, c and e), and the dimension ca. 21, 30 and 48 nm, respectively. The D_h of the micelles measured by DLS is larger than those observed by TEMs since the micelles are swollen in toluene, while TEM observation shows the dried. The TEMs of micelles containing gold nanoparticles are shown in Fig. 10b, d and f. Clearly, all hybrid micelles still keep spherical and narrowly distributing. The gold nanoparticles are uniformly dispersed into the core of the micelles and have small quantum dimension (2.5 ± 0.2 nm, 2.4 ± 0.3 nm and 2.0 ± 0.2 nm), identical particle morphology and narrow distribution. These data are obtained by over 50 dimensions of gold nanoparticles recorded on different locations of the TEM grid.

Generally, in the preparation process of the gold nanoparticles by PS-*b*-P4VP diblock copolymer, some other steps

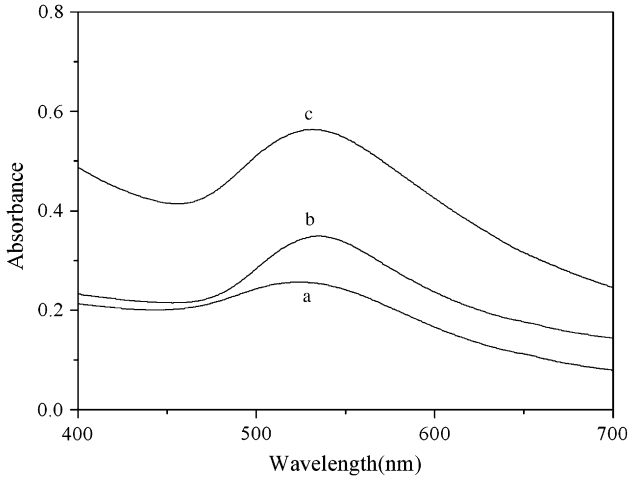

Fig. 9. UV–vis absorption spectra of gold nanoparticles prepared with complex micelles of: (a) $(PS_{25}$-*b*-$P4VP_{17})_4$, (b) $(PS_{25}$-*b*-$P4VP_{37})_4$ and (c) $(PS_{25}$-*b*-$P4VP_{63})_4$, where polymer concentration is 0.2 mg/mL and at 0.5 equiv of $HAuCl_4 \cdot 3H_2O$ per pyridine.

had to be introduced into this system for avoiding a broad size distribution of the particles caused by the aggregation of particles by induced collision [10,35]. For example, the micelle cores should be slightly cross-linked with *p*-xylene-dibromide (5% per 2VP) and small amounts of methanol was added into the micellar solution to provide a higher mobility of the inner micelle cores [35]. In this case, narrow distributed gold nanoparticles are obtained without any extra step. The reason is that the petal-like shell efficiently prohibits the hybrid micelles to coagulate. Compared to the single gold nanoparticles prepared by star-block copolymers PS-*b*-P2VP [13], in the present case, the gold nanoparticles have smaller size (ca. 2 nm). According to the experimental results of Schubert [14] and McFarland [15], the ratio of block length of shell to core has a great effect on the size of the gold nanoparticles. However, under our experimental condition, the obtained gold nanoparticles have a relatively uniform size at the different ratios of length of shell to core.

4. Conclusion

In this paper, low PDI $(PS$-*b*-$P4VP)_4$ with different length of P4VP chains are synthesized by two-step ATRP. The polymers form reverse micelles with P4VP as core and PS as petal-like shell in toluene. The reverse micelles and the micelles complex with $HAuCl_4 \cdot 3H_2O$ are investigated by means of dynamic laser scattering and static laser scattering. The results show that the size of core increases for micelles formed by $(PS_{25}$-*b*-$P4VP_{17})_4$ and $(PS_{25}$-*b*-$P4VP_{37})_4$ after incorporation with $HAuCl_4 \cdot 3H_2O$, while decreases for $(PS_{25}$-*b*-$P4VP_{63})_4$ owing to the competition between electrostatic repulsion and chelation. The petal-like shells efficiently stabilize the core–shell interface and prevent aggregation both for micelles and complex micelles at high R_g/R_h value. We have obtained small particle size (ca. 2 nm), identical particle morphology and narrow distribution by reducing the complex micelles with

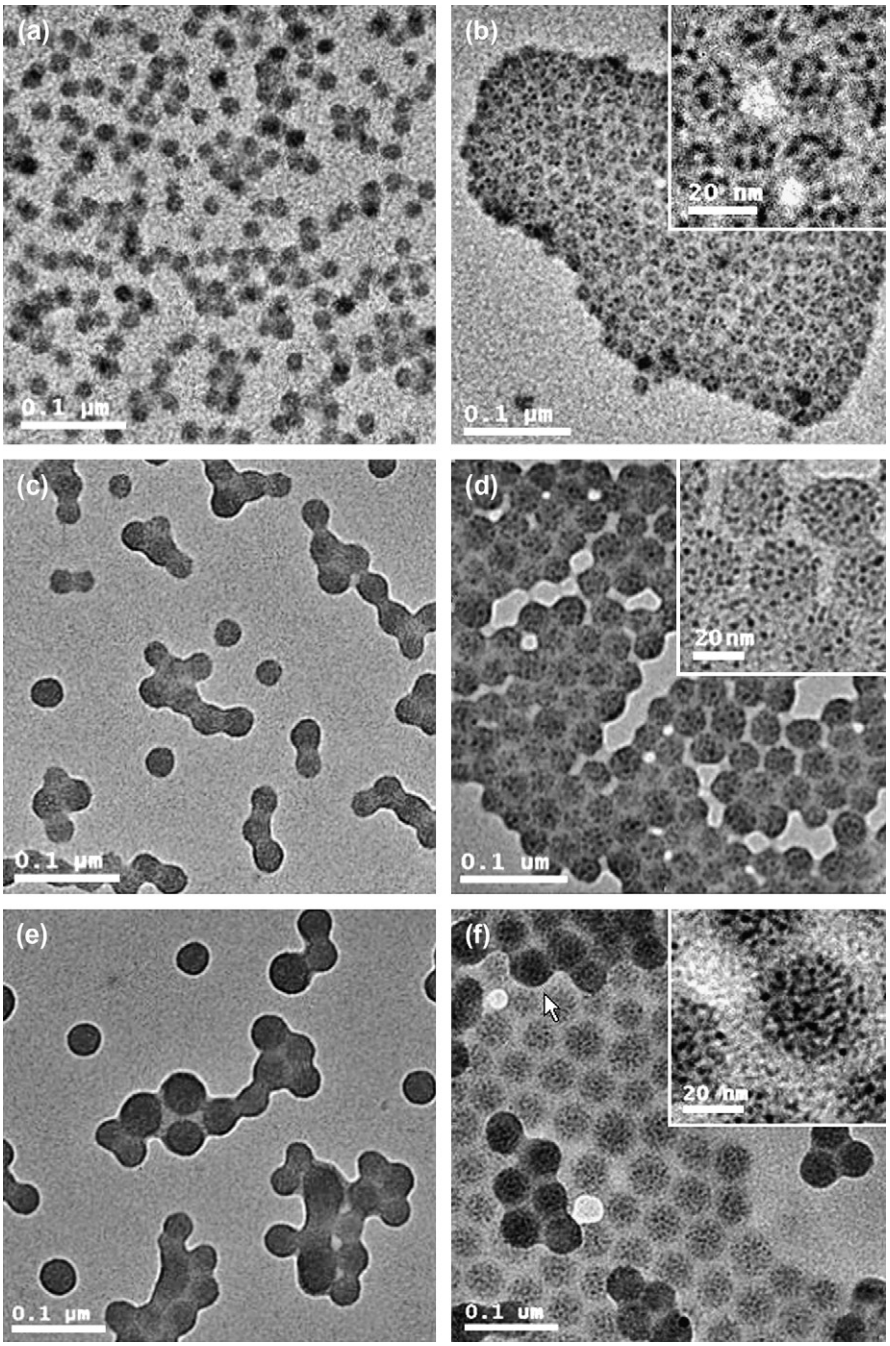

Fig. 10. TEM images of the micelles formed by: (a) $(PS_{25}$-*b*-$P4VP_{17})_4$ and (b) their gold nanoparticle, (c) $(PS_{25}$-*b*-$P4VP_{37})_4$ and (d) their gold nano particles, (e) $(PS_{25}$-*b*-$P4VP_{63})_4$ and (f) their gold nano particles. Where the polymers concentration are 0.1 mg/mL for the micelles and 0.2 mg/mL for the micelles containing gold nanoparticles.

anhydrous N_2H_4. The reverse micelles with petal-like shell have been confirmed to be ideal nanoreactors. The reverse micelles may also be a promising candidate used for drug delivery, stimuli responsive release, catalysis or phase transfer by changing the chain block.

Acknowledgment

This work was supported by the National Natural Science Foundation of China (No.20474032, 23030407), Specialized Research Fund for the Doctoral Program of Higher Education (No.20030055025) and Program for New Century Talents in Universities.

References

[1] Savic R, Luo L, Eisenberg A, Maysinger D. Science 2003;300:615.
[2] Kakizawa Y, Kataoka K. Adv Drug Delivery Rev 2002;54:203.
[3] Volkov AG. Interfacial catalysis. New York: Marcel Dekker; 2003.
[4] Holmberg K. Surfactants and polymers in aqueous solution. 2nd ed. Chichester: John Wiley & Sons; 2003.

[5] Förster S, Antoniett M. Adv Mater 1998;10:195.
[6] Sun S, Murray CB, Weller D, Folks L, Moser A. Science 2000;287:1989.
[7] Teranishi T, Haga M, Shiozawa Y, Miyake M. J Am Chem Soc 2000;122:4237.
[8] Jaramillo TF, Baeck SH, Cuenya BR, McFarland EW. J Am Chem Soc 2003;125:7148.
[9] Sidorov SN, Bronstein LM, Kabachii YA, Valetsky PM, Soo PL, Maysinger D, et al. Langmuir 2004;20:3543.
[10] Mössmer S, Spatz JS, Möller M, Aberle T, Schmidt J, Burchard W. Macromolecules 2000;33:4791.
[11] Spatz JP, Mössmer S, Hartmann C, Möller M. Langmuir 2000;16:407.
[12] Sun X, Dong S, Wang E. Polymer 2004;45:2181.
[13] Ho YJ, Park MK, Locklin J, Advincula R, Yang JH, Mays J. Langmuir 2002;18:2457.
[14] Filali M, Meier MAR, Schubert US, Gohy JF. Langmuir 2005;21:7995.
[15] Cuenya BR, Baeck SH, Jaramillo TF, McFarland EW. J Am Chem Soc 2003;125:12928.
[16] Kwee T, Taylor SJ, Mauritz KA, Storey RF. Polymer 2005;46:4480.
[17] Jin RH. Macromol Chem Phys 2003;204:403.
[18] Gauthier M, Li JM, Dockendorff J. Macromolecules 2003;36:2642.
[19] Zhang R, Liu J, Han B, Wang B, Sun D, He J. Polymer 2005;46:3936.
[20] Jeong YI, Nah JW, Lee HC, Kim SH, Cho CS. Int J Pharm 1999;188:49.
[21] Ciampolini M, Nardi N. Inorg Chem 1966;5:41.
[22] Matyjaszewski K, Miller PJ, Pyun J, Kickelbick G, Diamanti S. Macromolecules 1999;32:6526.
[23] Wang X, Zhang H, Shi M, Wang X, Zhou Q. J Polym Sci Part A Polym Chem 2005;43:733.
[24] (a) Zhang W, Shi L, An Y, Gao L, Wu K, Ma R, et al. Phys Chem Chem Phys 2004;6:109;
(b) Wu C, Fu J, Zhao Y. Macromolecules 2000;33:9040.
[25] Zhao Y, Shuai Xi, Chen C, Xi F. Macromolecules 2004;37:8854.
[26] Yu X, Tang X, Pan C. Polymer 2005;46:11149.
[27] Xu R, Winnik MA, Hallett FR, Riess G, Croucher MD. Macromolecules 1991;24:87.
[28] Calderara F, Riess G. Macromol Chem Phys 1996;197:2115.
[29] Förster S, Zisenis M, Wenz E, Antonietti M. J Chem Phys 1996;104:5996.
[30] (a) Chu B. Laser light scattering. 2nd ed. New York: Academic Press; 1991;
(b) Bantle S, Schmidt M, Burchard W. Macromolecules 1982;15:1604.
[31] (a) Wu C, Zuo J, Chu B. Macromolecules 1989;22:633;
(b) Antonietti M, Heinz S, Schimidt M. Macromolecules 1990;23:3796;
(c) Huber K, Bantle S, Lutz P, Burchard W. Macromolecules 1985;18:1461;
(d) Burchard W, Schmidt M, Stockmayer W. Macromolecules 1980;13:1265;
(e) Tu Y, Wan X, Zhang D, Zhou Q, Wu C. J Am Chem Soc 2000;122:10201;
(f) Zhang G, Liu L, Zhao Y, Ning F, Jiang M, Wu C. Macromolecules 2000;33:6340.
[32] Spatz JP, Sheiko S, Möller M. Macromolecules 1996;29:3220.
[33] Riess G. Prog Polym Sci 2003;28:1107.
[34] Mie G. Ann Phys 1908;25:377.
[35] Fendler JH. Nanoparticles and nanostructured film. Weinheim, Germany: Wiley-VCH; 1998.